Geophysical Research Letters

The Diurnal Nature of Future Extreme Precipitation Intensification

Edmund P. Meredith[1] (ID) **, Uwe Ulbrich[1]** (ID) **, and Henning W. Rust[1]**

[1]Institut für Meteorologie, Freie Universität Berlin, Berlin, Germany

Abstract Short-duration, high-impact precipitation events in the extratropics are invariably convective in nature, typically occur during the summer, and are projected to intensify under climate change. The occurrence of convective precipitation is strongly regulated by the diurnal convective cycle, peaking in the late afternoon. Here we perform very high resolution (convection-permitting) regional climate model simulations to study the scaling of extreme precipitation under climate change across the diurnal cycle. We show that the future intensification of extreme precipitation has a strong diurnal signal and that intraday scaling far in excess of overall scaling, and indeed thermodynamic expectations, is possible. We additionally show that, under a strong climate change scenario, the probability maximum for the occurrence of heavy to extreme precipitation may shift from late afternoon to the overnight/morning period. We further identify the thermodynamic and dynamic mechanisms which modify future extreme environments, explaining both the future scaling's diurnal signal and departure from thermodynamic expectations.

Plain Language Summary The most intense rainfall events—predominantly warm-season thunderstorms—are predicted to become more intense in a warmer climate. Thunderstorms occur most often in the late afternoon, at the peak of the diurnal convective cycle. How the future intensification of extreme rainfall events will interact with the diurnal convective cycle remains uncertain. Here we employ the newest generation of climate models—convection-permitting climate models—to study this question. Due to their high spatial resolution, convection-permitting models can directly simulate convective processes (which was not possible with older generations of climate models), making them an ideal tool for studying changes in intense thunderstorms. We find that the future intensification of intense rainfall events is not uniform across all hours of the day but instead has a strong diurnal signal, with the midmorning period seeing the greatest intensification. An implication of this diurnally unequal intensification is that under a strong climate change scenario the diurnal convective maximum for extremes may, in some regions, shift from late afternoon to the overnight/morning period.

1. Introduction

Both theory (Allen & Ingram, 2002; Fischer & Knutti, 2016; Trenberth, 1999) and models (Ban et al., 2015; Fischer & Knutti, 2016; Kendon et al., 2014; Prein et al., 2017) predict the intensification of extreme precipitation in response to a warming climate, continuing the observed trends of previous decades (Donat et al., 2013, 2016; Groisman et al., 2005). A first-principles estimate (Allen & Ingram, 2002; Trenberth, 1999) based on thermodynamic considerations places this intensification—often referred to as "trend scaling" (Zhang et al., 2017) or "future scaling"—at roughly 6.5% per degree of climate warming (Allen & Ingram, 2002; Ban et al., 2015); this follows from the Clausius-Clapeyron (CC) relation, which dictates that atmospheric saturation vapor pressure scales at this rate. Convection-permitting models (CPMs), that is, high-resolution models (grid spacing <4 km; Prein et al., 2015) which can explicitly simulate deep-convective processes, generally predict future scaling at close to the CC rate (Ban et al., 2015; Prein et al., 2017), though have also shown super-CC (Kendon et al., 2014; Knist et al., 2018) and sub-CC (Fosser et al., 2017) scaling signals in certain regions. Indeed, dynamic factors can exert strong control on regional future scaling rates and often feed back to either damp or amplify the thermodynamic signal (Emori & Brown, 2005; Pfahl et al., 2017; Shepherd, 2014). In particular, short-duration subdaily extremes may be susceptible to stronger scaling due to the higher sensitivity of convective dynamics to changes in temperature (Berg et al., 2013). Conversely, future scaling of precipitation extremes may be kept sub-CC in some regions due to future changes in moist
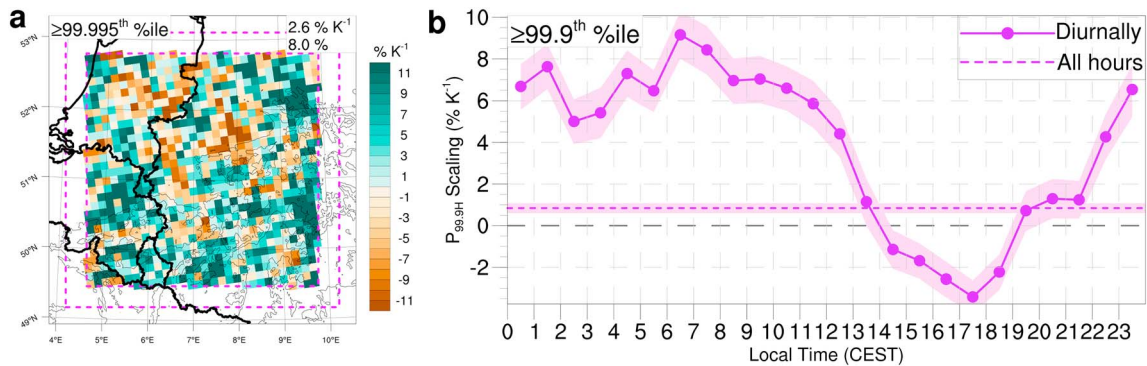
Figure 1. Scaling of hourly extreme precipitation and simulation domain. (a) Extreme hourly precipitation scaling (all hours ≥99.995th percentile) and model domain. Inner and outer dashed magenta lines mark the analysis region and the edge of the model relaxation zone, respectively. Area average scaling and change of extreme precipitation, statistically significant at the 0.01 level based on bootstrap resampling, are shown in the top right corner; contours mark model orography in 200-m steps. The simulation domain is centered over western Germany and also covers most of the Benelux region and parts of eastern France. (b) Diurnal cycle of extreme hourly precipitation scaling (all hours ≥99.9th diurnal hourly percentiles), area-averaged over the analysis region. Values are plotted in the middle of their 1-hr accumulation periods. Dashed line shows the equivalent scaling when all hours (≥99.9th all-hour percentile) are considered together. Shading denotes 95% confidence intervals determined via bootstrapping. See section 2 for details of how scaling is computed. All data are aggregated to the 12-km grid prior to analysis. CEST = Central European Summer Time.

adiabatic and environmental lapse rates (O'Gorman & Schneider, 2009; Prein et al., 2017), changes in vertical velocity statistics (O'Gorman & Schneider, 2009), and additionally, if the temperature at which peak precipitation occurs does not increase in parallel with changes in the mean temperature (O'Gorman & Schneider, 2009; Wang et al., 2017). Observed temperature-extreme precipitation relationships from the present-day climate—so-called "binning scaling" (Zhang et al., 2017)—are thus of limited utility in extrapolating future precipitation extremes (Ban et al., 2015; Chan et al., 2016; Prein et al., 2017; Wang et al., 2017).

Subdaily extreme precipitation during the extratropical summer is a leading cause of flash flooding and is almost exclusively convective. The diurnal convective cycle gives a late afternoon probability maximum for the occurrence of such events in the present climate. Whether the future scaling of extreme precipitation also has a diurnal component and how this may impact the diurnal convective cycle remains uncertain. Due to inadequate horizontal resolution, standard climate models cannot directly simulate most convective processes and must instead rely on convective parametrization schemes to fill this gap. Such models struggle to realistically represent subdaily extreme precipitation, producing extremes which are spatially too widespread, not locally intense enough, and temporally too persistent (Kendon et al., 2012). Crucially, convective parametrization schemes produce a diurnal convective maximum too early in the afternoon (Berthou et al., 2018; Hohenegger et al., 2008; Kendon et al., 2012; Prein et al., 2015). CPMs, however, correct the temporal bias in the diurnal convective cycle (Ban et al., 2014; Berthou et al., 2018; Hohenegger et al., 2008; Kendon et al., 2012; Prein et al., 2015), greatly improve the representation of precipitation extremes (Ban et al., 2014; Berthou et al., 2018; Kendon et al., 2012, 2014; Prein et al., 2015), and can even modify the climate change signal of their coarse-resolution forcing model (Kendon et al., 2017; Prein et al., 2015). CPMs are thus an ideal tool for investigating the future scaling of extreme precipitation at the diurnal scale, which has to date not been studied in detail.

To study future changes in extreme precipitation at the diurnal scale, as well as changes in the diurnal cycle, we perform regional climate model (RCM) simulations at convection-permitting resolution (2.2 km) for historical (1970–1999) and future (2070–2099) climates with the CCLM RCM (Rockel et al., 2008; see section 2 for details). We use the strongest future climate change scenario, Representative Concentration Pathway 8.5 (RCP8.5; Van Vuuren et al., 2011), and the general circulation model (GCM) is MPI-ESM-LR, which was continuously downscaled to 12-km resolution over Europe (Keuler et al., 2016). We further dynamically downscale these 12-km simulations (Keuler et al., 2016) to 2.2-km resolution from April to August each year, over a domain covering most of western Germany and the Benelux countries (Figure 1a). Analysis is focused on the summer months (June, July, August [JJA]), with April and May discarded for spin-up, and is performed at the spatial scale of the 12-km model. Lacking a large ensemble of GCM-RCM combinations, our aim is not to provide the definitive verdict on how extreme precipitation in our region will change but rather to explore plausible mechanisms by which changes may occur.

2. Data and Methods

2.1. RCM Simulations

We perform historical and future RCM simulations at convection-permitting resolution with the COSMO-CLM (CCLM) RCM (Rockel et al., 2008), version 4.8. CCLM is the community model of the German regional climate research community, jointly further developed by the CLM-Community (https://www.clm-community.eu/). Several previous studies have shown the CCLM run at convection-permitting resolution to provide an improved representation of both precipitation statistics and the diurnal cycle of summer convective precipitation, including in central Europe, compared to simulations at coarser resolutions requiring convective parametrization schemes (Ban et al., 2014; Berthou et al., 2018; Brisson et al., 2016; Fosser et al., 2015; Hackenbruch et al., 2016; Hohenegger et al., 2008; Langhans et al., 2013; Prein et al., 2013). Our simulation domain is centered over the Wupper catchment in western Germany (Figure 1a), a key research site of the BINGO project (http://www.projectbingo.eu/), and covers most of western Germany and the Benelux countries.

The modeling chain begins with the Max Planck Institute's global model, MPI-ESM-LR. As part of the CMIP5 project (Taylor et al., 2012), continuous transient runs were performed with MPI-ESM-LR using observed greenhouse gas concentrations from 1949 to 2005 (historical) and RCP8.5 (Van Vuuren et al., 2011) from 2006 to 2100 (Giorgetta et al., 2013). The CLM-Community continuously downscaled one MPI-ESM-LR member to 0.11° resolution (~12 km) with CCLM over the EURO-CORDEX domain (Keuler et al., 2016). We use CCLM to further downscale these 0.11° simulations to 0.02° resolution (~2.2 km) over our regional domain (Figure 1a) for the historical (1970–1999) and future (2070–2099) periods. Our simulations are 5-month time slices from 1 April to 31 August each year. The first two months of each time slice simulation are discarded for soil moisture spin-up, as in Ban et al. (2015). Analysis is thus focused on the summer months (JJA).

The 0.02° CCLM historical simulations show a secondary peak in the diurnal precipitation cycle at about 0700 CEST (Central European Summer Time; see section 3.2); this is a robust feature found both in observations in other regions (Hohenegger et al., 2008; Prein et al., 2013) and in observations (Weigl & Winterrath, 2009) in our region (Figure S1). The simulations used in this study are described in further detail in section 2.4 of Meredith et al. (2018).

2.2. Analyses

To increase the signal-to-noise ratio, all data from the 0.02° simulations are spatially aggregated to the 0.11° grid prior to analysis, giving over 25 model cells per analysis cell. We additionally restrict our analysis region to those areas sufficiently far from the lateral boundaries to allow the spin-up of small-scale features (Brisson et al., 2016; Figure 1a). Analysis is focused on extreme hourly precipitation during the summer months (JJA), at the diurnal scale. For each hour of day, extreme precipitation is defined as the average of all events exceeding the 99.9th percentile of hourly precipitation for that hour—equivalent to the top three events per hour of day. Empirical percentiles are computed using all (i.e., wet and dry) hours. Using empirical all-hour percentiles ensures an equal number of exceedances at each grid cell in each climate, which would not necessarily be the case for wet-hour percentiles or percentile estimates based on parametric distributions, for example, extreme value distributions. All-hour percentiles are additionally not prone to producing misleading results due to changes in wet-hour frequency, as is the case with wet-hour percentiles (Schär et al., 2016).

Scaling. To compute the extreme precipitation scaling under climate change—often referred to as "trend scaling" (Zhang et al., 2017) or "future scaling"—as shown in Figure 1, the percentage change in extreme precipitation intensity is divided by the climate change warming signal (K); this is done separately for each hour of day in Figure 1b. The extreme precipitation scaling curve presented in Figure 1b is the area average of the grid cell scalings across our analysis region, as opposed to the scaling of the area average precipitation; its diurnal variability is insensitive to the use of wet-hour or all-hour percentiles.

The temperature scaling curves—often referred to as "binning scaling" (Zhang et al., 2017)—for extreme convective available potential energy (CAPE) calculated for Figure 4b are computed as follows: for a given grid cell, all hours are assigned to overlapping temperature bins of 2 K width, with bin centers separated by 0.1 K. For each temperature bin, the empirical 99.5th percentile of CAPE is computed, producing a curve. To avoid adverse effects associated with inadequate sample size within the bins (Boessenkool et al., 2017), empirical percentiles are only computed when there are at least 200 data points within the temperature bin.
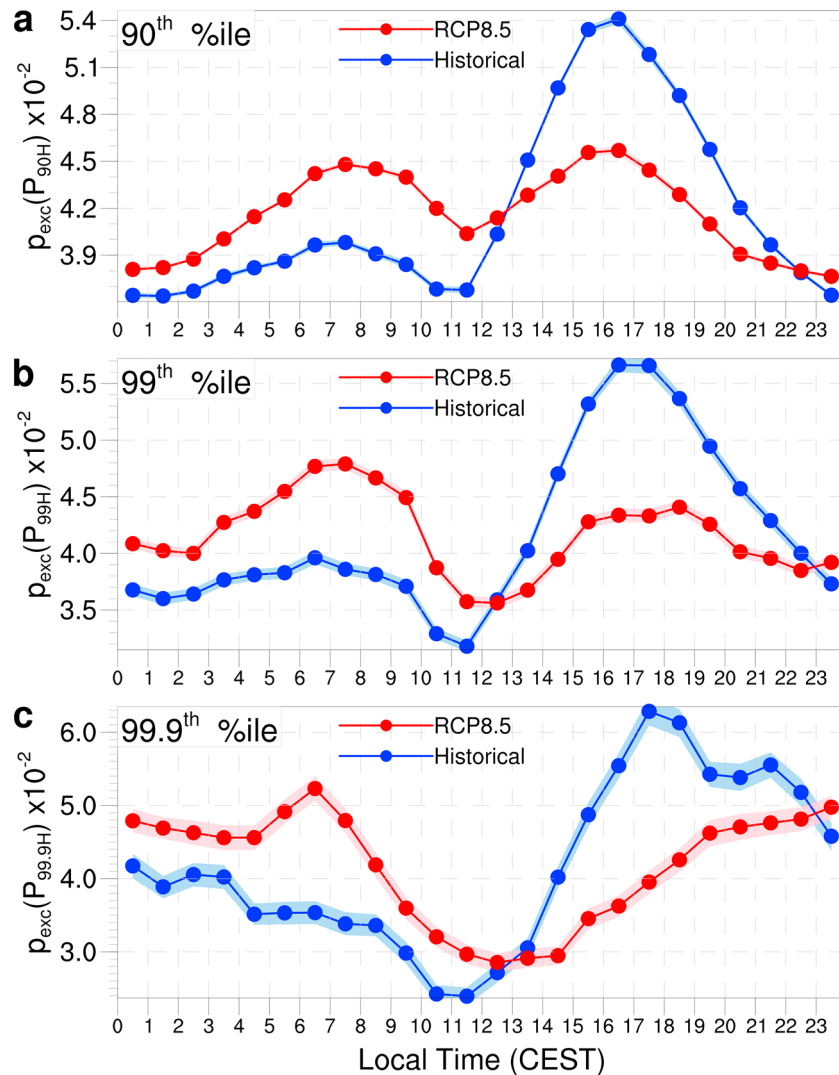
Figure 2. Exceedance probabilities. Future and historical probabilities that the (a) 90th, (b) 99th, and (c) 99.9th percentiles of *all* hours (i.e., not conditioned on the hour of day) will be exceeded during a given hour of the day. Percentiles are computed separately for each climate; curves represent area averages. Shading denotes 95% confidence intervals determined via bootstrapping. RCP8.5 = Representative Concentration Pathway 8.5. CEST = Central European Summer Time.

The area mean is then computed by averaging the curves of all grid cells (as long as at least 50% of the grid cells contain sufficient data to compute empirical percentiles) and applying a 15-point (1.5 K) smoothing. The temperature-precipitation curves presented in Figures S7 and S17 in the supporting information are computed in the same way, except with precipitation instead of CAPE.

Further analyses. To understand the diurnal scaling curves, we focus on the atmospheric properties accompanying the extremes—that is, exceedances of the diurnal hourly 99.9th percentiles—at each hour of day, at the grid cell in which an extreme precipitation event occurred. The temperatures in Figure 3a represent the 2-m temperatures at the start of the accumulation period. In the cases of CAPE and CIN in Figure 3, we consider the maximum value in the two hours up to the start of the precipitation accumulation period and also in directly adjacent grid cells. In Figure 4a, the changing probability that extreme 1700–1800 precipitation is accompanied by precipitation of a given magnitude at another time of the same day, and in the same region, is shown. For this, the maximum precipitation in a region of 9 × 9 grid cells, centered on the extreme cell, is first taken for all hours of the day on which the 1-hr extreme occurred. This is repeated for all 1700–1800 extremes across all cells, producing 24 separate probability distributions of precipitation (one
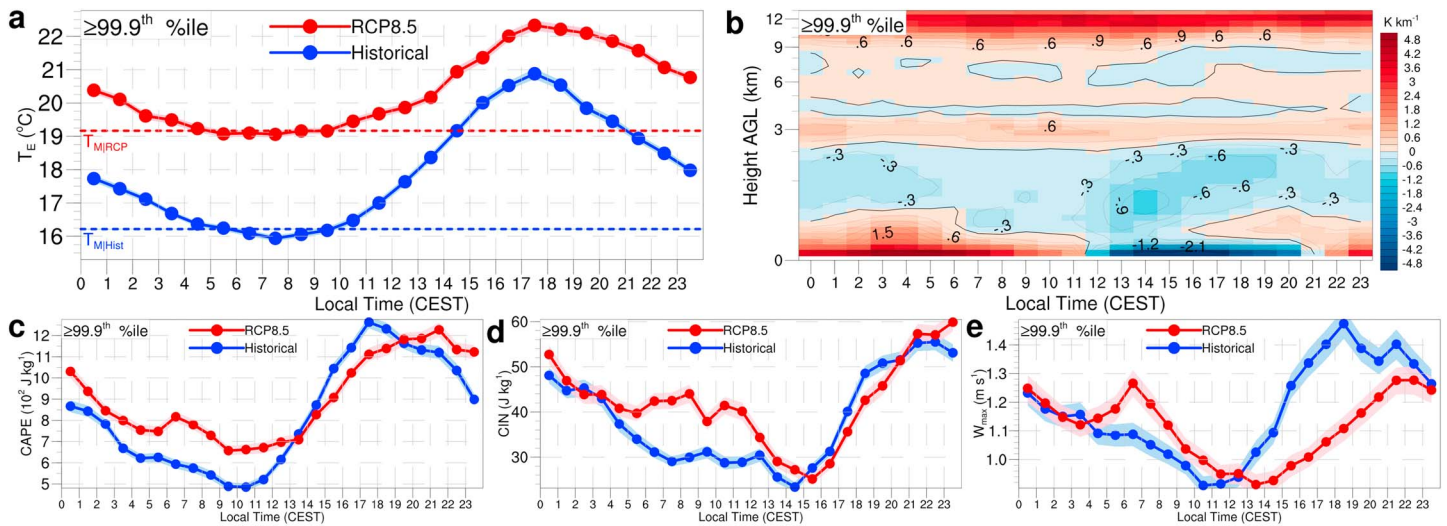
Figure 3. Extreme Environments. (a) Temperatures (2 m) accompanying diurnal precipitation extremes, at the start of the accumulation period. Straight dashed lines show the climatological mean temperatures (i.e., across all hours and not conditional on precipitation). (b) Future changes in conditional instability (CI; defined as environmental lapse rate-moist adiabatic lapse rate) accompanying extremes. Red (blue) shading signifies areas where environmental lapse rate decreases less (more) than MALR, thus increasing (decreasing) CI. (c) CAPE, (d) CIN, and (e) vertical velocity maxima accompanying historical and future extremes. CAPE and CIN values represent the most unstable parcel in the column. Vertical velocity maxima represent the maximum vertical velocity below 12 km. Shading denotes 95% confidence intervals determined via bootstrapping. See section 2 for further details of calculations. RCP8.5 = Representative Concentration Pathway 8.5; CAPE = convective available potential energy; CIN = convective inhibition; CEST = Central European Summer Time.

for each hour of the day; 2-mm bin widths). The historical distributions are then subtracted from the future distributions to produce Figure 4a.

Bootstrapping. The 95% confidence intervals of the area means are computed via bootstrap resampling (Efron & Tibshirani, 1994). For each area mean, the cells of the component 2-D field are randomly resampled with replacement to create a new 2-D field with the same number of cells, from which the mean is then recomputed. This is repeated 10,000 times to create a distribution of alternative area means. Following Davison and Hinkley (1997) the 95% basic bootstrap confidence intervals are then computed as $[2t - t^{*}_{q0.975}, 2t - t^{*}_{q0.025}]$, where t is the area mean and $t^{*}_{q[0.025|0.975]}$ are the [0.025|0.975] quantiles of the 10,000 estimates of the area mean. Pros, cons, and conceptual issues associated with the bootstrapping approach are additionally discussed in Hesterberg (2015).

Analyses were performed with NCAR (National Center for Atmospheric Research) Command Language (http://www.ncl.ucar.edu/, NCL (2017)), version 6.4.0, and R (https://www.R-project.org/, R Core Team (2017)).

3. Results
3.1. Extreme Precipitation Scaling at the Diurnal Scale

The overall scaling of extreme hourly precipitation (Figure 1a), that is, without conditioning the empirical percentiles on the hour of day, is taken as a baseline against which to compare the diurnal scaling. The strongest 0.005% of hourly precipitation—equivalent to the top three events across all 30 summers—shows an area mean increase of just 8.0% and consequently a sub-CC scaling (2.6%/K) averaged across our region, as in previous studies of adjacent regions (Fosser et al., 2017). Despite the characteristic lack of geographical structure at the grid cell scale, as also shown in, for example, Chan et al. (2014) and Ban et al. (2015), the area mean change is statistically significant at the 0.01 level. Distinguishing between different hours of the day (Figure 1b), it is however clear that the all-hour scaling is a poor guide to intraday scaling. Intraday scaling of hourly precipitation extremes in fact exhibits a strong diurnal component, with peak scaling in the morning and a late afternoon minimum. We note that the climate change warming signal exhibits a diurnal asymmetry (Davy et al., 2017); this cannot account for our findings (Figure S3). Within the diurnal scaling cycle, extreme precipitation scaling ranges from negative to super-CC, despite overall scaling being firmly sub-CC. Using extreme value theory, even stronger scaling can be found across the diurnal cycle for high return levels, exceeding twice the CC rate in the morning period (Figure S4). Interestingly, the minimum
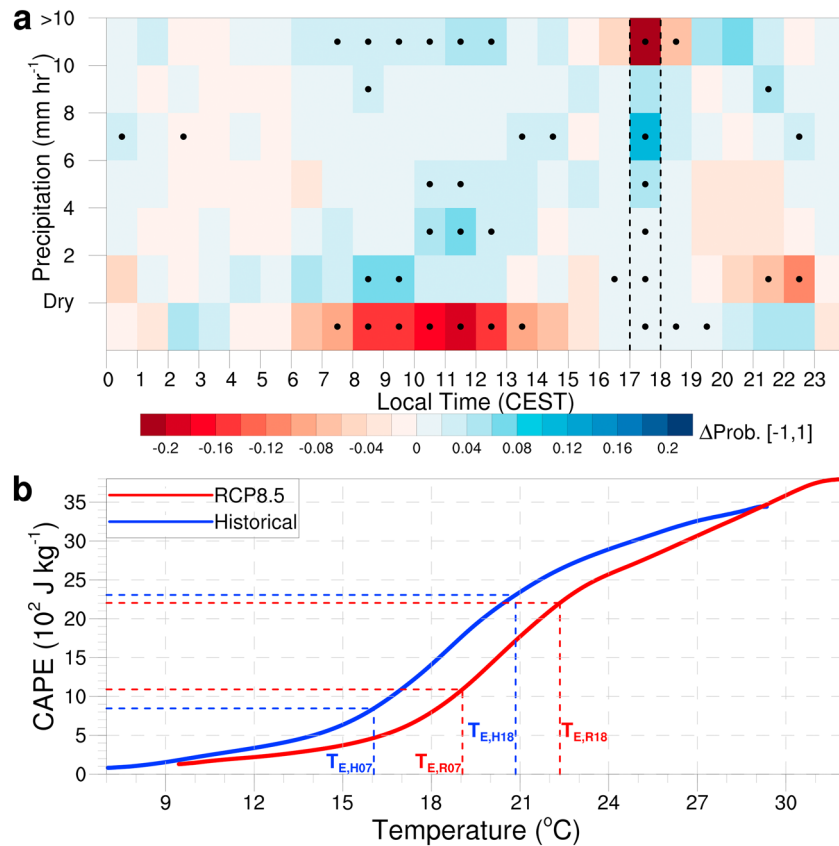
Figure 4. Drivers of changes. (a) Future change in probability that extreme 1700–1800 hourly precipitation is accompanied by precipitation of a given magnitude at a different time of the same day, within the region of the extreme; black dots mark changes statistically significant at the 0.05 level, based on 10,000 bootstrap resamples. (b) Historical and future temperature (2 m) scaling of extreme CAPE (99.5th percentile of hourly CAPE conditional on temperature bin). The 95% confidence intervals determined via bootstrapping are narrower than the thickness of the plotted curves and thus not visible. Blue and red dashed lines mark the mean temperatures of extremes (T_E), historical, and future, occurring at 0600–0700 and 1700–1800 local time (as shown in Figure 3a). See section 2 for full explanation of both computations. RCP8.5 = Representative Concentration Pathway 8.5; CAPE = convective available potential energy. RCP8.5 = Representative Concentration Pathway 8.5; CEST = Central European Summer Time.

of the diurnal scaling cycle comes in the late afternoon, the present climate time of day associated with the daily convective maximum (Figure 2). This negative scaling in the late afternoon is thus the dominant contributor to overall scaling being sub-CC.

3.2. Changing Diurnal Convective Cycle

The diurnal variation in the scaling of extreme precipitation (Figure 1b) has implications for the temporal occurrence probability of heavy to extreme precipitation during future scenario days (Figure 2). For light to moderate events, the future probability maximum remains in the late afternoon, though with a reduced probability. The future morning maximum, however, grows to almost equal the late afternoon probability maximum. As events become heavier, the pattern of decreasing probability in the late afternoon and increasing probability in the morning continues under the RCP8.5 scenario. By the 99.9th percentile of all hours—roughly equivalent to the two strongest events per summer—the late afternoon probability peak disappears and overnight/morning become the most probable periods for heavy precipitation thresholds to be exceeded (Figure 2c); this tendency continues toward more extreme percentiles (Figure S5). The collapse of the late afternoon peak seen at high percentiles in the RCP8.5 climate has no parallel in the historical period.

To understand the diurnally unequal scaling of extreme precipitation and the resultant changes in the diurnal occurrence probabilities of extremes, we examine the thermodynamic and dynamic environments within which the extremes are occurring. To this end, we focus on atmospheric conditions accompanying

exceedances of the *diurnal* 99.9th percentiles of hourly precipitation, equating to the top three events per hour of day at each grid cell.

3.3. Thermodynamic and Dynamic Environments

The temperature at which precipitation extremes occur (T_E) sets the upper limit on their environmental saturation humidity (Q_s). In the a.m. period, where scaling is strongest, future scenario T_E increases in line with changes in the mean temperature (T_M; Figure 3a)—roughly 3 K—meaning that Q_s preceding the extremes can scale with T_M. In the p.m. period, however, T_E increases by as little as 50% of the mean warming, meaning that pre-event Q_s cannot scale with T_M: sub-CC scaling thus results. Indeed, these temperature differences are evident throughout the lower troposphere (Figure S6). While the increase of T_M greatly exceeds that of T_E in the p.m. period, this difference can at best only partly account for the weak scaling rates found in the p.m. period, let alone explain the negative scaling in the late afternoon. In general, for a given climate the relationship between temperature and extreme precipitation has a peak-like structure: rainfall intensity falls off with higher temperatures when atmospheric moisture availability plateaus and column relative humidity thus decreases (Prein et al., 2017; Wang et al., 2017; Figure S7). Reduced relative humidity is thus often cited as a cause of decreasing precipitation intensity at high temperatures (Drobinski et al., 2016; Hardwick Jones et al., 2010). In our region, however, future changes in relative humidity preceding precipitation extremes do not mirror the diurnal scaling curve but rather enhance (reduce) relative humidity in the p.m. (a.m.) pre-extreme environment (Figure S8).

In addition to thermodynamic changes, the dynamic environment in which precipitation extremes occur strongly regulates their intensity. In particular, changes to the moist adiabatic and environmental lapse rates (MALR and ELR) can act to either damp or amplify the scaling of precipitation extremes (O'Gorman & Schneider, 2009). Stronger upper-tropospheric warming, for example, acts to reduce instability by curbing the buoyancy of parcels which have passed their level of free convection. Indeed, for convective regimes, stronger upper-tropospheric warming is a robust signal across climate models (Bony et al., 2006; Kotlarski et al., 2012). Once the ELR exceeds the MALR, the environment becomes conditionally unstable: with saturation or sufficient lift, air parcels will become unstable and potentially undergo deep convection if sufficient CAPE is present. It is thus not just changes in the ELR and MALR that are important but also their relative changes. We thus define the conditional instability (CI) as the difference ELR −MALR. Comparing the CI of the future and historical pre-extreme environments (Figure 3b), differential lapse rate changes act to strongly decrease (increase) near-surface CI in the p.m. (a.m) period, with the effect extending through much of the lower troposphere in the p.m. period. In both the historical and future periods, a.m. extreme environments are characterized by an absolutely stable layer (ELR < MALR) in the lower troposphere, acting to inhibit convective initiation (Figure S9). In the future period, however, this absolutely stable a.m. layer overlays a conditionally unstable layer that extends to the surface, which is not the case in the historical period.

The effects of the unequal lapse rate changes on the pre-extreme environments are manifested in a combination of both increased (decreased) CAPE and convective inhibition (CIN) preceding the future a.m. (p.m.) extremes (Figures 3c and 3d). CIN often contributes to more intense convection by allowing higher CAPE to build up before convective initiation (Figure S10). These changed dynamics result in more (less) intense vertical ascent (Figure 3e), total column moisture convergence, and hence, more (less) intense precipitation in the a.m. (p.m.) period (Figures S11 and S12).

3.4. Drivers of Changed Environments

Despite the future p.m. extremes occurring in both moister (relative and absolute) and warmer environments, we still see even negative scaling in the late afternoon period, highlighting the dominant role of the dynamic environment in the asymmetric a.m./p.m. scaling. Atmospheric developments earlier in the day can strongly influence the amplitude of the diurnal convective maximum. Morning convection, for example, can reduce the potential for intense convection the same afternoon (Fosser et al., 2017) by cooling the lower troposphere and removing instability. The relatively high convective activity of the future a.m. period appears to have this effect on the future p.m. extremes: on days when future p.m. extremes occur, there is a greatly increased probability that precipitation has already fallen in the region earlier that day, relative to the historical climate (Figure 4a) and contrary to the overall trend for more dry hours in the future (Figure S13). Similarly, wet mornings/early afternoons in the future period are much more likely to be followed by a late afternoon extreme percentile exceedance, in contrast to the reduced probability of being followed by a nonextreme wet event (Figure S14). The moistening of the lower atmosphere which follows from the

earlier precipitation explains the increased relative humidities (Figure S8) and lower temperature increases (Figures 3a and S6) which accompany the future p.m. extremes and also acts to reduce both CIN (important for avoiding premature convective initiation) and CAPE in their pre-extreme environments (Figures 3c and 3d). See Text S1 (supporting information) for further elucidation of these relationships.

Another important factor in the reduced convective potential we find for the future p.m. extremes is a non-stationary relationship between near-surface temperature and high CAPE values. In general, the highest CAPE extremes are found in the presence of high near-surface temperatures (Rasmussen et al., 2017). This relationship, however, changes between the historical and future climates (Figure 4b), which is attributable to the vertically unequal climate change signal of tropospheric warming (Figure S15). For the temperature range in which heavy precipitation typically occurs, a higher near-surface temperature is required in the future climate to achieve a given CAPE value, sometimes as much as 2 K higher (Figure 4b). The future a.m. extremes, in which T_E increases by roughly 3 K, can overcome this nonstationarity to still achieve higher CAPE values than their historical counterparts, contributing to their super-CC scaling. In the p.m. period, however, the increase in T_E is more modest and the nonstationarity thus yields the lower CAPE values which accompany the negatively scaling p.m. extremes. While unconditional CAPE extremes (i.e., not conditional on extreme precipitation) in the future are stronger than in the historical climate, these CAPE extremes tend to occur in moisture limited environments and thus cannot be realized as precipitation extremes (Figures S16 and S17).

4. Discussion

Our results demonstrate that, under a strong climate change scenario, there exists the potential for a temporal shift in the diurnal distribution of extreme summertime precipitation: the present-day late afternoon peak may recede in favor of the overnight/morning period. The potential societal impacts of summertime precipitation extremes preferentially occurring during such hours merit consideration. The time of emergence for detectable changes in summertime hourly precipitation extremes is likely to be well into the second half of the current century (Kendon et al., 2018), though potentially sooner than for changes in summertime daily precipitation extremes in our study region (Maraun, 2013). Projected changes may also be sensitive to GCM-RCM combinations, albeit recent evidence suggests that climatologies (Berthou et al., 2018) and climate change signals (Kendon et al., 2017) of extreme hourly JJA precipitation from models with different parametrizations and dynamical cores may converge with increasing resolution. While our findings cannot simply be extrapolated to other regions of the globe, extratropical regions in which T_M increase considerably outstrips that of late afternoon T_E have the potential for similar effects. Separate CPM climate simulations over the European Alps (Ban et al., 2015) also exhibit a diurnal scaling cycle (not shown). Our results additionally suggest that future changes in certain instability indexes (e.g., Diffenbaugh et al., 2013; Púčik et al., 2017) may not be reliable predictors of future changes in extreme precipitation, as this approach assumes both a stationary index-temperature relation and T_E scaling with T_M and thus does not account for the availability of moisture to feed developing storms at higher temperatures. We conclude by emphasizing that the higher moisture levels which are possible in a warmer climate do not necessarily translate into CC-scaled precipitation extremes across the diurnal cycle. On the contrary, the (often opposing) influences of dynamics and moisture availability vary across the diurnal cycle to produce a range of scalings, thus necessitating a holistic analysis of future extremes and their environments, which can be best achieved with CPMs.

References

Allen, M. R., & Ingram, W. J. (2002). Constraints on future changes in climate and the hydrologic cycle. *Nature*, *419*(6903), 224–232.

Ban, N., Schmidli, J., & Schär, C. (2014). Evaluation of the convection-resolving regional climate modeling approach in decade-long simulations. *Journal of Geophysical Research: Atmospheres*, *119*, 7889–7907. https://doi.org/10.1002/2014JD021478

Ban, N., Schmidli, J., & Schär, C. (2015). Heavy precipitation in a changing climate: Does short-term summer precipitation increase faster? *Geophysical Research Letters*, *42*, 1165–1172. https://doi.org/10.1002/2014GL062588

Berg, P., Moseley, C., & Haerter, J. O. (2013). Strong increase in convective precipitation in response to higher temperatures. *Nature Geoscience*, *6*(3), 181–185.

Berthou, S., Kendon, E. J., Chan, S. C., Ban, N., Leutwyler, D., Schär, C., & Fosser, G. (2018). Pan-european climate at convection-permitting scale: A model intercomparison study. *Climate Dynamics*, 1–25.

Boessenkool, B., Bürger, G., & Heistermann, M. (2017). Effects of sample size on estimation of rainfall extremes at high temperatures. *Natural Hazards and Earth System Sciences*, *17*(9), 1623–1629. Retrieved from https://www.nat-hazards-earth-syst-sci.net/17/1623/2017/note=https://doi.org/10.5194/nhess-17-1623-2017

Bony, S., Colman, R., Kattsov, V. M., Allan, R. P., Bretherton, C. S., Dufresne, J.-L., et al. (2006). How well do we understand and evaluate climate change feedback processes? *Journal of Climate*, *19*(15), 3445–3482.

Brisson, E., Demuzere, M., & van Lipzig, N. P. M. (2016). Modelling strategies for performing convection-permitting climate simulations. *Meteorologische Zeitschrift*, *25*(2), 149–163.

Brisson, E., Van Weverberg, K., Demuzere, M., Devis, A., Saeed, S., Stengel, M., & van Lipzig, N. P. (2016). How well can a convection-permitting climate model reproduce decadal statistics of precipitation, temperature and cloud characteristics? *Climate Dynamics*, *47*(9-10), 3043–3061.

Chan, S., Kendon, E., Fowler, H., Blenkinsop, S, & Roberts, N. (2014). Projected increases in summer and winter UK sub-daily precipitation extremes from high-resolution regional climate models. *Environmental Research Letters*, *9*(8), 084019.

Chan, S. C., Kendon, E. J., Roberts, N. M., Fowler, H. J., & Blenkinsop, S. (2016). Downturn in scaling of UK extreme rainfall with temperature for future hottest days. *Nature Geoscience*, *9*(1), 24–28.

Davison, A. C., & Hinkley, D. V. (1997). *Bootstrap methods and their application*, vol. 1. Cambridge: Cambridge university press.

Davy, R., Esau, I., Chernokulsky, A., Outten, S., & Zilitinkevich, S. (2017). Diurnal asymmetry to the observed global warming. *International Journal of Climatology*, *37*(1), 79–93.

Diffenbaugh, N. S., Scherer, M., & Trapp, R. J. (2013). Robust increases in severe thunderstorm environments in response to greenhouse forcing. *Proceedings of the National Academy of Sciences*, *110*, 16,361–16,366.

Donat, M., Alexander, L., Yang, H, Durre, I, Vose, R, Dunn, R., et al. (2013). Updated analyses of temperature and precipitation extreme indices since the beginning of the twentieth century: The HadEX2 dataset. *Journal of Geophysical Research: Atmospheres*, *118*, 2098–2118. https://doi.org/10.1002/jgrd.50150

Donat, M. G., Lowry, A. L., Alexander, L. V., OGorman, P. A., & Maher, N. (2016). More extreme precipitation in the worlds dry and wet regions. *Nature Climate Change*, *6*(5), 508–513.

Drobinski, P., Alonzo, B., Bastin, S., Silva, N. D., & Muller, C. (2016). Scaling of precipitation extremes with temperature in the french mediterranean region: What explains the hook shape? *Journal of Geophysical Research: Atmospheres*, *121*, 3100–3119. https://doi.org/10.1002/2015JD023497

Efron, B., & Tibshirani, R. J. (1994). An introduction to the bootstrap, *Monographs on Statistics and Applied Probability* (Vol. 57). Boca Raton: CRC press.

Emori, S., & Brown, S. (2005). Dynamic and thermodynamic changes in mean and extreme precipitation under changed climate. *Geophysical Research Letters*, *32*, L17706. https://doi.org/10.1029/2005GL023272

Fischer, E. M., & Knutti, R. (2016). Observed heavy precipitation increase confirms theory and early models. *Nature Climate Change*, *6*(11), 986–991.

Fosser, G., Khodayar, S., & Berg, P. (2015). Benefit of convection permitting climate model simulations in the representation of convective precipitation. *Climate Dynamics*, *44*(1-2), 45–60.

Fosser, G, Khodayar, S, & Berg, P. (2017). Climate change in the next 30 years: What can a convection-permitting model tell us that we did not already know?. *Climate Dynamics*, *48*(5-6), 1987–2003.

Giorgetta, M. A., Jungclaus, J., Reick, C. H., Legutke, S., Bader, J., Böttinger, M., et al. (2013). Climate and carbon cycle changes from 1850 to 2100 in MPI-ESM simulations for the coupled model intercomparison project phase 5. *Journal of Advances in Modeling Earth Systems*, *5*, 572–597. https://doi.org/10.1002/jame.20038

Groisman, P. Y., Knight, R. W., Easterling, D. R., Karl, T. R., Hegerl, G. C., & Razuvaev, V. N. (2005). Trends in intense precipitation in the climate record. *Journal of Climate*, *18*(9), 1326–1350.

Hackenbruch, J., Schädler, G., & Schipper, J. W. (2016). Added value of high-resolution regional climate simulations for regional impact studies. *Meteorologische Zeitschrift*, *25*, 291–304.

Hardwick Jones, R., Westra, S., & Sharma, A. (2010). Observed relationships between extreme sub-daily precipitation, surface temperature, and relative humidity. *Geophysical Research Letters*, *37*, L22805. https://doi.org/10.1029/2010GL045081

Hesterberg, T. C. (2015). What teachers should know about the bootstrap: Resampling in the undergraduate statistics curriculum. *The American Statistician*, *69*(4), 371–386.

Hohenegger, C., Brockhaus, P., & Schaer, C. (2008). Towards climate simulations at cloud-resolving scales. *Meteorologische Zeitschrift*, *17*(4), 383–394.

Kendon, E. J., Ban, N., Roberts, N. M., Fowler, H. J., Roberts, M. J., Chan, S. C., et al. (2017). Do convection-permitting regional climate models improve projections of future precipitation change? *Bulletin of the American Meteorological Society*, *98*(1), 79–93.

Kendon, E. J., Blenkinsop, S., & Fowler, H. J. (2018). When will we detect changes in short-duration precipitation extremes? *Journal of Climate*, *31*(7), 2945–2964.

Kendon, E. J., Roberts, N. M., Fowler, H. J., Roberts, M. J., Chan, S. C., & Senior, C. A. (2014). Heavier summer downpours with climate change revealed by weather forecast resolution model. *Nature Climate Change*, *4*(7), 570–576.

Kendon, E. J., Roberts, N. M., Senior, C. A., & Roberts, M. J. (2012). Realism of rainfall in a very high-resolution regional climate model. *Journal of Climate*, *25*(17), 5791–5806.

Keuler, K., Radtke, K., Kotlarski, S., & Lüthi, D. (2016). Regional climate change over europe in COSMO-CLM: Influence of emission scenario and driving global model. *Meteorologische Zeitschrift*, *25*(2), 121–136.

Knist, S., Goergen, K., & Simmer, C. (2018). Evaluation and projected changes of precipitation statistics in convection-permitting WRF climate simulations over central europe. *Climate Dynamics*, 1–17.

Kotlarski, S., Bosshard, T., Lüthi, D., Pall, P, & Schär, C. (2012). Elevation gradients of european climate change in the regional climate model COSMO-CLM. *Climatic Change*, *112*(2), 189–215.

Langhans, W., Schmidli, J., Fuhrer, O., Bieri, S., & Schär, C. (2013). Long-term simulations of thermally driven flows and orographic convection at convection-parameterizing and cloud-resolving resolutions. *Journal of Applied Meteorology and Climatology*, *52*(6), 1490–1510.

Maraun, D. (2013). When will trends in European mean and heavy daily precipitation emerge? *Environmental Research Letters*, *8*(1), 014004.

Meredith, E. P., Rust, H. W., & Ulbrich, U. (2018). A classification algorithm for selective dynamical downscaling of precipitation extremes. *Hydrology and Earth System Sciences*, *22*(8), 4183–4200. Retrieved from https://www.hydrol-earth-syst-sci.net/22/4183/2018/, https://doi.org/10.5194/hess-22-4183-2018

Meredith, E. P., Ulbrich, U., & Rust, H. W. (2019). Bingo wupper 0.02 degree climate simulations. World Data Center for Climate (WDCC) at DKRZ. Retrieved from http://cera-www.dkrz.de/WDCC/ui/Compact.jsp?acronym=DKRZLTA_961_ds00006

NCL (2017). The NCAR Command Language (Version 6.4.0) [Software]. (2017). Boulder, Colorado: UCAR/NCAR/CISL/TDD. https://doi.org/10.5065/D6WD3XH5. Retrieved from http://www.ncl.ucar.edu/

O'Gorman, P. A., & Schneider, T. (2009). Scaling of precipitation extremes over a wide range of climates simulated with an idealized GCM. *Journal of Climate*, *22*(21), 5676–5685.

Pfahl, S., OGorman, P. A., & Fischer, E. M. (2017). Understanding the regional pattern of projected future changes in extreme precipitation. *Nature Climate Change*, *7*(6), 423–427.

Prein, A. F., Gobiet, A., Suklitsch, M., Truhetz, H., Awan, N., Keuler, K., & Georgievski, G. (2013). Added value of convection permitting seasonal simulations. *Climate Dynamics*, *41*(9-10), 2655–2677.

Prein, A. F., Langhans, W., Fosser, G., Ferrone, A., Ban, N., Goergen, K., et al. (2015). A review on regional convection-permitting climate modeling: Demonstrations, prospects, and challenges. *Reviews of Geophysics*, *53*, 323–361. https://doi.org/10.1002/2014RG000475

Prein, A. F., Rasmussen, R. M., Ikeda, K., Liu, C., Clark, M. P., & Holland, G. J. (2017). The future intensification of hourly precipitation extremes. *Nature Climate Change*, *7*(1), 48–52.

Púčik, T., Groenemeijer, P., Rädler, A. T., Tijssen, L., Nikulin, G., Prein, A. F., et al. (2017). Future changes in european severe convection environments in a regional climate model ensemble. *Journal of Climate*, *30*(17), 6771–6794.

R Core Team (2017). R: A language and environment for statistical computing. [Computer software manual]. Vienna, Austria. Retrieved from https://www.R-project.org/

Rasmussen, K., Prein, A., Rasmussen, R., Ikeda, K, & Liu, C. (2017). Changes in the convective population and thermodynamic environments in convection-permitting regional climate simulations over the United States. *Climate Dynamics*, 1–26.

Rockel, B., Will, A., & Hense, A. (2008). The regional climate model COSMO-CLM (CCLM). *Meteorologische Zeitschrift*, *17*(4), 347–348.

Schär, C., Ban, N., Fischer, E. M., Rajczak, J., Schmidli, J., Frei, C., et al. (2016). Percentile indices for assessing changes in heavy precipitation events. *Climatic Change*, *137*(1-2), 201–216.

Shepherd, T. G. (2014). Atmospheric circulation as a source of uncertainty in climate change projections. *Nature Geoscience*, *7*, 703–708.

Taylor, K. E., Stouffer, R. J., & Meehl, G. A. (2012). An overview of CMIP5 and the experiment design. *Bulletin of the American Meteorological Society*, *93*(4), 485–498.

Trenberth, K. E. (1999). Conceptual framework for changes of extremes of the hydrological cycle with climate change. *Climatic Change*, *42*(1), 327–339.

Van Vuuren, D. P., Edmonds, J., Kainuma, M., Riahi, K., Thomson, A., Hibbard, K., et al. (2011). The representative concentration pathways: An overview. *Climatic Change*, *109*(1-2), 5–31.

Wang, G., Wang, D., Trenberth, K. E., Erfanian, A., Yu, M., Bosilovich, M. G., & Parr, D. T. (2017). The peak structure and future changes of the relationships between extreme precipitation and temperature. *Nature Climate Change*, *7*(4), 268–274.

Weigl, E., & Winterrath, T. (2009). Radargestützte Niederschlagsanalyse und-vorhersage (RADOLAN, RADVOR-OP). *Promet*, *35*, 78–86.

Zhang, X., Zwiers, F. W., Li, G., Wan, H., & Cannon, A. J. (2017). Complexity in estimating past and future extreme short-duration rainfall. *Nature Geoscience*, *10*(4), 255–259.